

We are IntechOpen, the world's leading publisher of Open Access books Built by scientists, for scientists

6,900

Open access books available

185,000

International authors and editors

200M

Downloads

Our authors are among the

154

Countries delivered to

TOP 1%

most cited scientists

12.2%

Contributors from top 500 universities



WEB OF SCIENCE™

Selection of our books indexed in the Book Citation Index
in Web of Science™ Core Collection (BKCI)

Interested in publishing with us?
Contact book.department@intechopen.com

Numbers displayed above are based on latest data collected.
For more information visit www.intechopen.com



Resonance Compression of Acoustic Beams in Crystals

*Vladimir I. Alshits, Dmitrii A. Bessonov
and Vasilii N. Lyubimov*

Abstract

The resonant excitation of an intense elastic wave through nonspecular reflection of a special pump wave in a crystal is described. Geometric criteria are found under which mode conversion, when the incident and reflected beams belong to different acoustic branches, coexists with total internal reflection of an acoustic beam. In this case, the entire energy of an incident pump wave is spent on the excitation of a narrow intense reflected beam close in structure to an eigenmode. A consistent choice of orientations of the sagittal plane and crystal surface that excludes the reflection of a parasitic wave of leakage is found. The resonance parameters have been found for a medium with an arbitrary anisotropy. General relations are concretized for monoclinic, orthorhombic, trigonal, tetragonal, cubic, and hexagonal systems. Estimates and illustrations are given for a series of such crystals. The intensity of the reflected beam increases with its narrowing, but its diffraction divergence also increases with this narrowing. Nevertheless, the intensity of the beam can be increased by a factor of 5–10 at sufficiently high frequencies while keeping its divergence at an acceptable level. Amplification by two orders of magnitude can be achieved by compressing the beam in two dimensions through its double reflection.

Keywords: crystals, elastic waves, acoustic beams, total internal reflection, mode conversion, efficiency of transformation, diffraction divergence

1. Introduction

Modern crystal acoustics is an important base for numerous instruments and devices using concentrated ultra- and hypersonic beams, delay lines, surface and bulk waves, etc. Many of acoustic effects in crystals arise exclusively due to their anisotropy. In particular, piezoelectricity exists only in crystals and is widely used in acoustic devices [1, 2]. Another spectacular example of a nontrivial role of anisotropy is phonon focusing [3], the concentration of energy in a crystal along special directions for which the acoustic beam in Poynting vectors is much narrower than that in wave vectors. In this chapter, we will consider another principle of energy concentration in acoustic waves that is also entirely related to crystal anisotropy. Intense ultrasonic beams are widely used in engineering, medicine, scientific instrument making, etc. [4]. The reflection and refraction of such beams at the interfaces between layered isotropic structures are commonly used for their transformation. Crystals open up new opportunities for beam transformation.

A method for producing intense beams in crystals based on the features of their elastic anisotropy was proposed in our paper [5]. “Compression” of an acoustic beam is achieved by choosing the geometry of the beam incidence on a surface close to the angle of total internal reflection, when one of the reflected beams ($r2$) propagates at a small angle to the surface (**Figure 1a**) and, its width can be made arbitrarily small. However, we need the compression not of the beam width, but of its energy density. For instance, in isotropic medium, a compression of such beam is accompanied by a decreasing amount of energy entering it, without any growth of its intensity. The same occurs in the crystal without a special choice of reflection geometry. And still in anisotropic media, there are specific orientations which admit the beam intensification.

As is shown in [5], this happens when the wave field of the beam $r2$ is close to the eigenmode—an exceptional bulk wave (EBW) satisfying the free surface boundary condition [6, 7]. The perturbation of the selected EBW propagation geometry transforms this one-partial solution to the resonance reflection component. To obtain such a special resonance reflection near the eigenmode, the EBW should exist on the middle sheet of the slowness surface, while the incident “pump” wave should belong to the external sheet (**Figure 1b**). The proper cuts can be found almost in any crystal. However, one should bear in mind that in this case, apart from the reflected wave $r2$ excited from the middle sheet of the slowness surface, another reflected wave $r1$ belonging to the external sheet inevitably exists. Energy losses related to this parasitic wave can be minimized by choosing crystals or geometries with parameters corresponding to the closeness of reflection to mode conversion, when such a parasitic wave does not appear.

In [5, 8], we considered perturbed geometries, where the surface of the crystal remained unchanged and the plane of reflection (sagittal plane) was rotated by a small angle φ about the normal \mathbf{n} to the surface (**Figure 1a**). In this case, an increase in the intensity of excited beam was controlled by the angle φ , whereas the energy loss to the parasitic beam was completely determined by the relation between the moduli of elasticity and could be reduced only by an appropriate choice of the crystal.

In [9], we analyzed another variant of the theory where a similar resonance in a hexagonal crystal was governed by the angle of rotation of the surface about the direction of propagation of the unperturbed exceptional bulk wave. In this case, conversion also occurs only under a certain relation between moduli of elasticity.

In [10, 11], the more general analysis was accomplished which allowed us to demonstrate that the mode conversion of resonance near total internal reflection (i.e., the scheme in **Figure 1a** without the parasitic beam $r1$) can be implemented in almost any acoustic crystal by a consistent variation of orientations of both the boundary and the sagittal planes.

In this chapter, we shall summarize the results of mentioned and some other studies of ours and present the combined theoretical consideration of the problem with both analytical approximate calculations and numerical exact computations

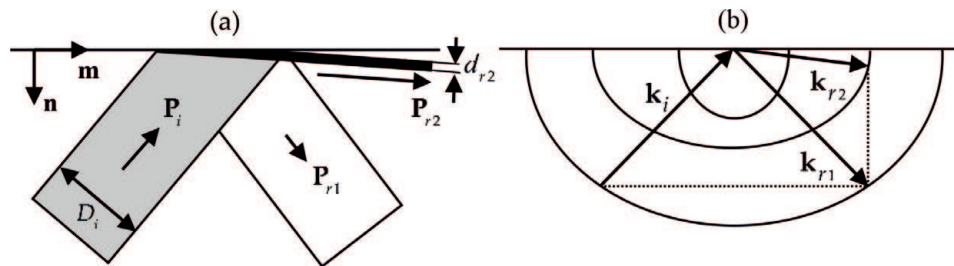


Figure 1. Scheme of excitation of a narrow beam near total internal reflection in the r space (a) and k space (b) with \mathbf{P}_i , \mathbf{k}_i ; \mathbf{P}_{r1} , \mathbf{k}_{r1} ; and \mathbf{P}_{r2} , \mathbf{k}_{r2} to be mean Poynting and wave vectors of the incident, parasitic, and excited beams, respectively.

checking the established relations between the basic parameters determining the unusual resonance phenomenon with features quite promising for applications.

2. Formulation of the problem and basic relations

Consider a semi-infinite elastic medium of unrestricted anisotropy with a free boundary. It will be characterized by the tensor of moduli of elasticity c_{ijkl} and the density ρ . The sagittal plane is specified by two unit vectors: the propagation direction \mathbf{m} along the surface and the normal \mathbf{n} to the surface. Reflection shown schematically in **Figure 1b** is the superposition of four partial waves: the incident ($\alpha = 4 = i$) and reflected ($\alpha = 1 = r1$) waves from the outer sheet of the slowness surface, the reflected wave ($\alpha = 2 = r2$) from the middle sheet, and the localized wave ($\alpha = 3 = l$) from the internal sheet:

$$\begin{pmatrix} \mathbf{u}(\mathbf{r}, t) \\ (i/k)\hat{\sigma}(\mathbf{r}, t) \end{pmatrix} = \sum_{\alpha=1}^4 C_{\alpha} \begin{pmatrix} \mathbf{A}_{\alpha} \\ \mathbf{L}_{\alpha} \end{pmatrix} \exp \{i(\mathbf{k}_{\alpha} \cdot \mathbf{r} - \omega t)\}. \quad (1)$$

Here, \mathbf{u} is the wave field displacement vector, $\hat{\sigma}$ is the stress tensor, C_{α} are the partial waves amplitudes, ω is the frequency, and $\mathbf{k}_{\alpha} = k(\mathbf{m} + p_{\alpha}\mathbf{n})$ are the wave vectors of partial components with a common projection k onto the direction of propagation \mathbf{m} (**Figure 1b**). The k value determines the tracing speed $v = \omega/k$ of stationary motion of the wave field (1) along the boundary. Vectors \mathbf{A}_{α} and \mathbf{L}_{α} characterize the partial field polarizations. Being not independent (as well as \mathbf{u} and $\hat{\sigma}$), these vectors are normalized by the condition: $\mathbf{A}_{\alpha}^2 = 1$.

In terms of Eq. (1), the boundary condition of free surface, $\sigma_{ij}n_j|_{y=0} = 0$, takes the form:

$$C_{r1}\mathbf{L}_1 + C_{r2}\mathbf{L}_2 + C_l\mathbf{L}_3 + C_i\mathbf{L}_4 = 0. \quad (2)$$

The unknown vectors \mathbf{A}_{α} and \mathbf{L}_{α} are found from the so-called Stroh's formalism based on the fact that the combined six-vectors $\xi_{\alpha} = \{\mathbf{A}_{\alpha}, \mathbf{L}_{\alpha}\}^T$ (the superscript T means transposition) together with parameters p_{α} ($\alpha = 1, \dots, 6$) are eigenvectors and eigenvalues of the 6×6 Stroh matrix \hat{N} [12],

$$\hat{N} = - \begin{pmatrix} (nn)^{-1}(nm) & (nn)^{-1} \\ (mn)(nn)^{-1}(nm) - (mm) - \rho v^2 \hat{I} & (mn)(nn)^{-1} \end{pmatrix}. \quad (3)$$

Here \hat{I} is the unit 3×3 matrix and the matrices (ab) are defined by the convolutions $(ab)_{jk} = a_i c_{ijkl} b_l$ of the moduli tensor c_{ijkl} with the vectors \mathbf{a} and \mathbf{b} . The six eigenvectors ξ_{α} are complete and orthogonal to each other everywhere apart from points of degeneracy. The orthogonality property may be expressed in the form:

$$\mathbf{A}_{\alpha} \cdot \mathbf{L}_{\beta} + \mathbf{A}_{\beta} \cdot \mathbf{L}_{\alpha} = 0, \quad \alpha \neq \beta. \quad (4)$$

Depending on v , the vectors ξ_{α} and the parameters p_{α} may be real or form complex conjugated pairs. The reflection considered in this chapter (**Figure 1b**) belongs to the second supersonic region of the slowness surface. In the above terms, here the wave superposition formally may include four bulk partial waves with real parameters p_{α} , two incident and two reflected, from the external and middle sheets. In addition, at our disposal, there are two inhomogeneous partial waves with complex conjugated parameters p_{α} , one localized and the other nonphysical (increasing into the depth of the medium), related to the internal sheet. The second incident wave and

the nonphysical inhomogeneous component were naturally excluded ($C_5 = C_6 = 0$) from the sums in Eqs. (1) and (2).

The amplitude C_i of the incident wave is assumed to be known, while the remaining amplitudes may be expressed in terms of C_i through scalar multiplication of Eq. (2) by the vector products $\mathbf{L}_2 \times \mathbf{L}_3$, $\mathbf{L}_1 \times \mathbf{L}_3$, or $\mathbf{L}_1 \times \mathbf{L}_2$. As a result, we arrive at the following reflection coefficients in the form of the ratios of mixed products:

$$R_1 = \frac{C_{r1}}{C_i} = -\frac{[\mathbf{L}_4 \mathbf{L}_2 \mathbf{L}_3]}{[\mathbf{L}_1 \mathbf{L}_2 \mathbf{L}_3]}, \quad R_2 = \frac{C_{r2}}{C_i} = \frac{[\mathbf{L}_4 \mathbf{L}_1 \mathbf{L}_3]}{[\mathbf{L}_1 \mathbf{L}_2 \mathbf{L}_3]}. \quad (5)$$

3. Singular reflection geometry in the vicinity of EBW

The deduced equations (5) represent just exact relations which describe the discussed resonance reflection only in some definite narrow region of orientations of surface and sagittal plane. Let us demonstrate that such singular region really arises close to the geometry of EBW propagation related to the pair $\{\mathbf{n}_0, \mathbf{m}_0\}$. Indeed, wave superposition (1) in this exceptional geometry is decomposed into two independent solutions—EBW and three-partial reflection—satisfying the boundary conditions, which are fragments of Eq. (2):

$$\mathbf{L}_{02} = 0, \quad (6)$$

$$C_{r1}\mathbf{L}_{01} + C_i\mathbf{L}_{03} + C_i\mathbf{L}_{04} = 0, \quad (7)$$

where the subscript 0 indicates the initial unperturbed configuration. Of course, near this geometry, the vector \mathbf{L}_2 should be small and the other vectors \mathbf{L}_1 , \mathbf{L}_3 , and \mathbf{L}_4 nearly coplanar. As a result, both the numerator and denominator of the expression for R_2 in (5) should independently approach zero; i.e., R_2 is singular. This singularity is responsible for the resonance character of reflection and, therefore, for the discussed effect. The coefficient R_1 in (5) is regular because the small vector \mathbf{L}_2 appears in both the denominator and the numerator of the expression for this coefficient.

Let us introduce practically important characteristics of the investigated resonance, specifically, the gain of excited wave intensity (K_2) and energy loss (K_1) in a parasitic wave:

$$K_2 = \frac{P_2}{P_4} = |R_2|^2 \frac{s_2}{s_4}, \quad K_1 = \frac{P_1}{P_4} = |R_1|^2 \frac{s_1}{s_4}. \quad (8)$$

Here, P_α are the Poynting vector lengths, which are products of the energy density in the corresponding partial wave ($\propto C_\alpha^2$) and its ray speed s_α . Another useful characteristic of the resonance is the excitation efficiency $\eta = 1 - K_1$, equal to the fraction of energy transferred from the incident to excited wave.

Thus, a small perturbation of the crystal orientation in the vicinity of the geometry of the EBW propagation may provide a resonance intensification of the reflected wave r_2 . The control parameters of resonance are the optimized characteristics of geometry of reflection $\{\mathbf{n}, \mathbf{m}\}$ (**Figure 1a**), i.e., the orientations of the surface and sagittal plane, as well as the angle of incidence α of the pump wave i related to these characteristics. The perturbation $\{\mathbf{n}_0, \mathbf{m}_0\} \rightarrow \{\mathbf{n}, \mathbf{m}\}$ is shown in **Figure 2a**. The new plane boundary P of the crystal is specified by the unit normal $\mathbf{n} = \mathbf{n}(\psi, \chi)$ rotated by a small angle $\psi = \angle(\mathbf{n}, \mathbf{n}_0)$ with respect to the normal \mathbf{n}_0 to the initial boundary P_0 along which the EBW can propagate. The axis of rotation

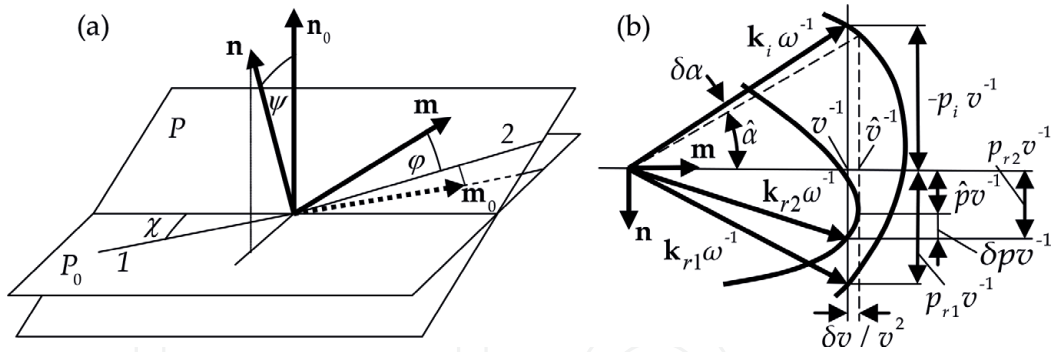


Figure 2. (a) Perturbations of the crystal surface $P_0 \rightarrow P$, its normal orientation $\mathbf{n}_0 \rightarrow \mathbf{n}$ and the propagation direction $\mathbf{m}_0 \rightarrow \mathbf{m}$; (b) the scheme of the resonance reflection (only outer and middle sheets of the slowness surface are shown).

(the intersection line between P and P_0 planes) is specified by the angle χ , counting from reference line $1 \parallel \mathbf{m}_0$ and lying in the range of $[0, \pi]$. The direction \mathbf{m} in the P plane is specified by the angle φ measured from line 2 along the projection of the unperturbed vector \mathbf{m}_0 on the boundary P .

Below, to compact equations, we will also use the alternative notation for the introduced small angles:

$$\phi_1 = \varphi, \quad \phi_2 = \psi. \quad (9)$$

In fact, as we shall see, the squares of these angles (in units of radians) rather than the angles themselves are small parameters in the theory developed below.

As is seen in **Figure 2b**, where the scheme of resonance reflection is shown, the angle α of incidence must be chosen near the threshold angle of total internal reflection $\hat{\alpha}$: $\alpha = \hat{\alpha} + \delta\alpha$. This configuration is characterized by the tracing speed $v = \omega/k$ of the wave field close to the limiting velocity \hat{v} . The adjusting angle $\delta\alpha$ controlling reflection resonance is directly related to the difference $\delta v = v - \hat{v} \approx \delta p^2 / 2\kappa$ [8]:

$$\delta\alpha = \frac{\delta v}{\hat{v}} A = \frac{A}{2\kappa\hat{v}} \delta p^2, \quad A = \frac{\hat{v}}{1 + p_i^2} \left(\frac{\partial p_i}{\partial v} \right)_{v=\hat{v}}, \quad (10)$$

where κ is the radius of curvature of the cross section of the middle sheet of the slowness surface by the sagittal plane at the limiting point corresponding to $v = \hat{v}$.

4. Analytical description of resonance characteristics

In this section, we shall obtain approximate expressions for the coefficients K_1 and K_2 defined by Eq. (8) in the general case of arbitrary anisotropy. Reflectivities R_1 and R_2 are expressed in (5) in terms of vectors \mathbf{L}_α , which will be considered as functions of the parameters δp , φ , ψ , and χ (see **Figure 2**). The last (not small) angle χ , which determines the axis for \mathbf{n} rotation, is considered fixed at this stage. Its influence on the effect will be studied numerically. Expressions (5) can be expanded in the other small parameters.

Given (7), the numerator in Eq. (5) for R_2 can be approximately represented as:

$$[\mathbf{L}_4 \mathbf{L}_1 \mathbf{L}_3] \approx \phi_i \left(\frac{\partial}{\partial \phi_i} [\mathbf{L}_4 \mathbf{L}_1 \mathbf{L}_3] \right)_0, \quad (11)$$

where the subscript 0 means that after differentiation, one should put $\phi = \psi = 0$, $\delta p = 0$.

To calculate the denominator in the expressions for reflection coefficients R_1 and R_2 (5), let us expand the two cofactors separately:

$$\mathbf{L}_3 \times \mathbf{L}_1 \approx \mathbf{L}_{03} \times \mathbf{L}_{01} + \phi_i \left(\frac{\partial}{\partial \phi_i} [\mathbf{L}_3 \times \mathbf{L}_1] \right)_0, \quad (12)$$

$$\mathbf{L}_2 \approx \phi_i \left(\frac{\partial \mathbf{L}_2}{\partial \phi_i} \right)_0 + \frac{1}{2} \phi_i \phi_j \left(\frac{\partial^2 \mathbf{L}_2}{\partial \phi_i \partial \phi_j} \right)_0 + \delta p \left(\frac{\partial \mathbf{L}_2}{\partial p_2} \right)_0. \quad (13)$$

In writing (13), we used the fact that $\mathbf{L}_{02} = 0$ (6). Substituting Eqs. (12) and (13) into the denominators of ratios (5), it is easy to verify that the term linear in ϕ and ψ drops out of the result. This term is proportional to the mixed product, which is zero,

$$\left[\mathbf{L}_{03} \mathbf{L}_{01} \left(\frac{\partial \mathbf{L}_2}{\partial \phi_i} \right)_0 \right] = 0, \quad (14)$$

because, as we will see, it is composed of coplanar vectors. Let us prove that they are all perpendicular to the same real vector \mathbf{A}_{02} . From orthogonality condition (4), one has

$$\mathbf{A}_{02} \cdot \mathbf{L}_{0\alpha} + \mathbf{L}_{02} \cdot \mathbf{A}_{0\alpha} = \mathbf{A}_{02} \cdot \mathbf{L}_{0\alpha} = 0. \quad (15)$$

for all $\alpha \neq 2$ where the fact that $\mathbf{L}_{02} = 0$ was again used.

In order to prove that the derivative $(\partial \mathbf{L}_2 / \partial \phi_i)_0$ is also orthogonal to \mathbf{A}_{02} , one can use identity $\mathbf{A}_2(\hat{v}) \cdot \mathbf{L}_2(\hat{v}) = 0$ valid for any transonic states of arbitrary geometry $\{\mathbf{m}, \mathbf{n}\}$ [13]. Let us differentiate this identity and then set $\phi = \psi = 0$:

$$\left(\mathbf{A}_2 \cdot \frac{\partial \mathbf{L}_2}{\partial \phi_i} + \mathbf{L}_2 \cdot \frac{\partial \mathbf{A}_2}{\partial \phi_i} \right)_0 = \mathbf{A}_{02} \cdot \left(\frac{\partial \mathbf{L}_2}{\partial \phi_i} \right)_0 = 0. \quad (16)$$

Thus, Eqs. (15) and (16) prove vanishing in (14), which means that indeed the denominator of both reflection coefficients (5) does not contain terms linear in ϕ and ψ . The numerator of R_1 is found from the same relations (12) and (13) after replacing in them indices $1 \rightarrow 4$, and the numerator of R_2 is given by Eq. (11). After some straightforward calculations, one obtains

$$R_1 = -\frac{F^{(4)} \delta p + G_{ij}^{(4)} \phi_i \phi_j}{F^{(1)} \delta p + G_{ij}^{(1)} \phi_i \phi_j}, \quad R_2 = \frac{H_i \phi_i}{F^{(1)} \delta p + G_{ij}^{(1)} \phi_i \phi_j}, \quad (17)$$

where the repeated subscripts imply summation, and the new notations are introduced:

$$F^{(\alpha)} = \left[\mathbf{L}_\alpha \frac{\partial \mathbf{L}_2}{\partial p_2} \mathbf{L}_3 \right]_0, \quad H_i = \left(\frac{\partial}{\partial \phi_i} [\mathbf{L}_4 \mathbf{L}_1 \mathbf{L}_3] \right)_0, \quad (18)$$

$$G_{ij}^{(\alpha)} = \left[\frac{\partial \mathbf{L}_2}{\partial \phi_i} \cdot \frac{\partial (\mathbf{L}_3 \times \mathbf{L}_\alpha)}{\partial \phi_j} + \frac{1}{2} \left(\mathbf{L}_\alpha \frac{\partial^2 \mathbf{L}_2}{\partial \phi_i \partial \phi_j} \mathbf{L}_3 \right) \right]_0. \quad (19)$$

For further compactness of expressions, let us also denote:

$$G_{ij}^{(\alpha)}/F^{(\alpha)} = \lambda_{ij}^{(\alpha)} \equiv \lambda'_{ij}^{(\alpha)} + i\lambda''_{ij}^{(\alpha)}, \quad H_i/F^{(1)} = \mu_i. \quad (20)$$

The substitution of Eq. (17) in terms of (20) into Eq. (8) gives

$$K_1 = \frac{s_1}{s_4} \left| \frac{F^{(4)}}{F^{(1)}} \right|^2 \frac{(\delta p + \lambda'_{ij}^{(4)} \phi_i \phi_j)^2 + (\lambda''_{ij}^{(4)} \phi_i \phi_j)^2}{(\delta p + \lambda'_{ij}^{(1)} \phi_i \phi_j)^2 + (\lambda''_{ij}^{(1)} \phi_i \phi_j)^2}, \quad (21)$$

$$K_2 = \frac{(\mu_i \phi_i)^2 s_2 / s_4}{(\delta p + \lambda'_{ij}^{(1)} \phi_i \phi_j)^2 + (\lambda''_{ij}^{(1)} \phi_i \phi_j)^2}. \quad (22)$$

As could be expected, loss coefficient K_1 (21) is regular in the control parameters φ , ψ , and δp , whereas gain K_2 (22) is singularly dependent on them: at $\phi_i \phi_j \ll \delta p \ll 1$, K_2 tends to zero, and at $\delta p \ll \phi_i \phi_j \ll 1$, it diverges.

5. Optimization of control parameters of reflection

Until now, we were free with a choice of geometry of the considered resonance reflection. It looks natural to choose the parameters φ , ψ , and δp so that the loss coefficient K_1 would be as small as possible, i.e., the efficiency η would be close to 100%. In terms of **Figure 1**, this means an exclusion of the parasitic reflected beam $r1$ which is equivalent to a realization of the mode conversion. Formula (21) allows reducing the criterion of conversion $K_1 = 0$ to the system of equations:

$$\lambda''_{ij}^{(4)} \phi_i \phi_j = 0, \quad \delta p = -\lambda'_{ij}^{(4)} \phi_i \phi_j, \quad (23)$$

where the first equation determines the relation between the angles of rotation of the sagittal plane ($\phi_1 \equiv \varphi$) and the normal to the surface ($\phi_2 \equiv \psi$) at a fixed position (χ) of the axis of rotation of the vector \mathbf{n} (see **Figure 2a**). The second equation in (23) at the found relation between φ and ψ specifies the dependence $\delta p(\varphi)$ and, by (10), the incidence angle $\delta\alpha(\varphi)$.

The first requirement in (23) is reduced to a quadratic equation with respect to the ratio ψ/φ . The existence of real roots of this equation (and, therefore, mode conversion) is generally not guaranteed. However, numerical calculations for a number of crystals of different symmetry systems did not give us examples of the absence of such roots. Furthermore, as is shown in the next section, for hexagonal crystals, this equation always has real roots for the case $c_{44} > c_{66}$. Thus, in many crystals, the consistent variation of orientations of the surface and sagittal plane really can provide the mode conversion near the total internal reflection, i.e., the effect which is under consideration.

The general conditions of mode conversion (23) can be represented in the compact form:

$$\psi = \gamma_{\pm} \varphi, \quad \delta p = \lambda_{\pm} \varphi^2. \quad (24)$$

These conditions with real roots γ_{\pm} specify two variants of the orientations of the surface, sagittal plane, and angle of incidence (for each angle χ , see **Figure 2a**) that ensure the energy concentrating in the reflected beam $r2$.

As was expected, the gain K_2 given by Eq. (22) should obviously be large because it is inversely proportional to the square of the small parameter:

$$K_2^{\text{con}} \propto \varphi^{-2} \propto \psi^{-2}. \quad (25)$$

But the unlimited increase in (25) with a decrease in the angle φ should not mislead us. Indeed, an increase in the amplitude (25) of the resonance peak (22) is accompanied by its narrowing. However, when this width in angles of incidence $\delta\alpha$ becomes smaller than the natural diffraction divergence of the beam, the further approach of the incident wave to the total internal reflection angle becomes senseless. Instead of the energy concentrating in the reflected beam r_2 , the more and more fraction of the incident beam will be out of resonance. Thus, a small divergence of the both beams proves to be an important requirement which, in turn, limits a permissible sound frequency ν from below. Let us estimate these limitations.

In the case of total mode conversion, the condition for the balance of energy fluxes in the incident and reflected beams has the form $P_i D_i = P_{r2} d_{r2}$ (**Figure 1a**). This balance gives

$$K_2^{\text{con}} \equiv P_{r2}/P_i = D_i/d_{r2}, \quad (26)$$

i.e., the reflected beam turns out to be narrower than the incident one by a factor of K_2 . On the other hand, the related diffraction divergence angles, $\delta_i \sim c_s/\nu D_i$ and $\delta_{r2} \sim c_s/\nu d_{r2}$ (where $c_s \sim 10^5$ cm/s is the sound speed), are in similar proportion:

$$\delta_{r2} \approx \frac{D_i}{d_{r2}} \delta_i = K_2^{\text{con}} \delta_i. \quad (27)$$

Thus, the possible increase in the coefficient K_2 is limited by the diffraction divergence of the r_2 beam. To decrease this divergence, the frequency ν must be high. The simple estimation gives the following characteristic values: at $\nu \sim 100$ MHz and $D \sim 1$ cm, one can obtain a coefficient $K_2 \sim 5\text{--}10$ at $d_{r2} \approx 1\text{--}2$ mm, $\delta_i \sim 10^{-3}$, and $\delta_{r2} \sim 10^{-2}$ rad.

For a fixed direction of the normal $\mathbf{n}(\psi, \chi)$ to the crystal boundary, the surfaces $K_2(\varphi, \delta\alpha)$ and $\eta(\varphi, \delta\alpha)$ have specific “ridges” (**Figure 3**). They are determined by the special extremal relations between the angles φ and $\delta\alpha$. In framework of our approximate theory [8] (see Section 6), these trajectories coincide and are described by the relation of the type $\delta\alpha = C\varphi^4$. And along the ridges, one obtains

$$K_2^{\text{max}} = \text{const}/\sqrt{\delta\alpha}, \quad \eta^{\text{max}} = \text{const}. \quad (28)$$

Of course, with variations of \mathbf{n} , the constants in (28) also change. For some definite direction of \mathbf{n} , the mode conversion occurs when $\eta^{\text{max}} = \eta^{\text{con}} = 1$ and $K_2^{\text{max}} = K_2^{\text{con}}$.

Unfortunately, the obtained identity of the extremal trajectories is just the consequence of our approximations. As numerical analysis shows, usually they are close but not identical. And on one of them, we deal with the mode conversion, $\eta^{\text{con}} = 1$ and K_2^{con} , whereas on the other, an increased extremal gain $K_2^{\text{max}} > K_2^{\text{con}}$ and a decreased efficiency $\eta^{\text{max}} < 1$ occur. It is even more important that on the second trajectory, the same value of coefficient K_2 is obtained at a larger angle $\delta\alpha$. And the numerical analysis shows that one can significantly increase $\delta\alpha$ in this case at the expense of a relatively small decrease in the efficiency η .

In **Figure 3** and in further considerations, we illustrate the performed analysis by numerical calculations for the series of crystals of various symmetry systems. The parameters of the resonance are calculated by exact formulas (5) and (8). We also vary the angle χ and do not limit ourselves to small angles φ and ψ .

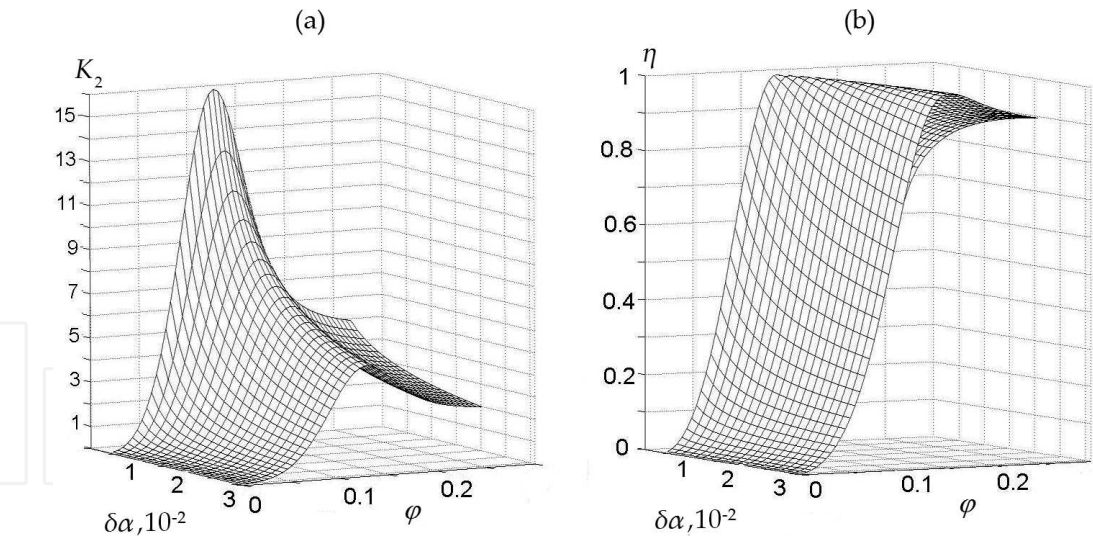


Figure 3. Numerical plot of surfaces $K_2(\varphi, \delta\alpha)$ (a) and $\eta(\varphi, \delta\alpha)$ (b) for graphite crystal with the fixed boundary parallel to the hexad axis 6; the φ angle is counted from the vector $\mathbf{m}_0 \perp 6$.

Systems	Crystal	$\mathbf{m}_0, \mathbf{n}_0$	Normal \mathbf{n}		φ_m, rad	$\delta\alpha_m, \text{rad}$	$\eta, \%$
			χ, rad	ψ, rad			
Cubic	LiF	$\mathbf{m}_0 \parallel \mathbf{x}', \mathbf{n}_0 \parallel \mathbf{y}'$	0.21	0.29	0.13	0.008	88.7
	Silicon		0.29	0.29	0.13	0.007	74.0
Hexagonal	Graphite	$\mathbf{m}_0 \parallel \mathbf{x}, \mathbf{n}_0 \parallel \mathbf{y}$	0	0.02	0.14	0.034	94.9
	ZnS		0.03	0.48	0.32	0.008	93.4
	CdCe		0.03	0.69	0.14	0.008	95.2
Tetragonal	Paratellurite	$\mathbf{m}_0 \parallel \mathbf{x}', \mathbf{n}_0 \parallel \mathbf{y}'$	0.09	0.03	0.07	0.013	99.8
	BaTiO ₃	$\mathbf{m}_0 \parallel \mathbf{x}, \mathbf{n}_0 \parallel \mathbf{z}$	0.05	0.28	0.37	0.031	80.0
Trigonal	Quartz	$\mathbf{m}_0 \parallel \mathbf{x}_1, \mathbf{n}_0 \parallel \mathbf{y}$	0.01	0.60	0.48	0.043	75.0
	LiNbO ₃	$\mathbf{m}_0 \parallel \mathbf{x}_2, \mathbf{n}_0 \parallel \mathbf{y}$	0.30	0.78	0.09	0.007	79.0
Orthorhombic	Rochelle salt	$\mathbf{m}_0 \parallel \mathbf{z}, \mathbf{n}_0 \parallel \mathbf{x}$	0.12	0.44	0.55	0.009	94.6
		$\mathbf{m}_0 \parallel \mathbf{x}, \mathbf{n}_0 \parallel \mathbf{z}$	0.18	0.47	-0.08	0.010	98.4

The unperturbed orientations of vectors \mathbf{m}_0 and \mathbf{n}_0 are determined by the axes x, y , and z of crystallographic coordinates, the bisector axes \mathbf{x}' and \mathbf{y}' in the basal plane xy and by the directions $\mathbf{x}_\alpha \parallel (\cos \theta_\alpha, 0, \sin \theta_\alpha)$, where $\theta_1 = -0.76$ and $\theta_2 = 0.46$ rad.

Table 1. Characteristics of extremal resonances $K_2 = 5$ for acoustic crystals of various symmetry systems.

Table 1 demonstrates the results of such analysis for a number of acoustic crystals. We present the geometries related to the extremal gains. The angles $\varphi_m, \psi_m, \chi_m$ and $\delta\alpha_m$ are found for the gains $K_2^{\max} = 5$. In the presented examples, the compromise choice of the extremal geometry, instead of mode conversion one, indeed leads to a substantial increase in adjusting angles $\delta\alpha_m$ with efficiency η_m retained rather high level. The magnitudes of $\delta\alpha_m$ remain fairly small (~ 0.01 rad on average) even after the compromise but still look to be acceptable for an experiment. On the other hand, for quartz, graphite, and BaTiO₃ crystals, the angle $\delta\alpha_m$ is several times larger than the mentioned mean values. In the case of graphite, the mentioned compromise leads to the increase of the tuning angle by a factor of 1.5 via reducing the efficiency η by only 5%.

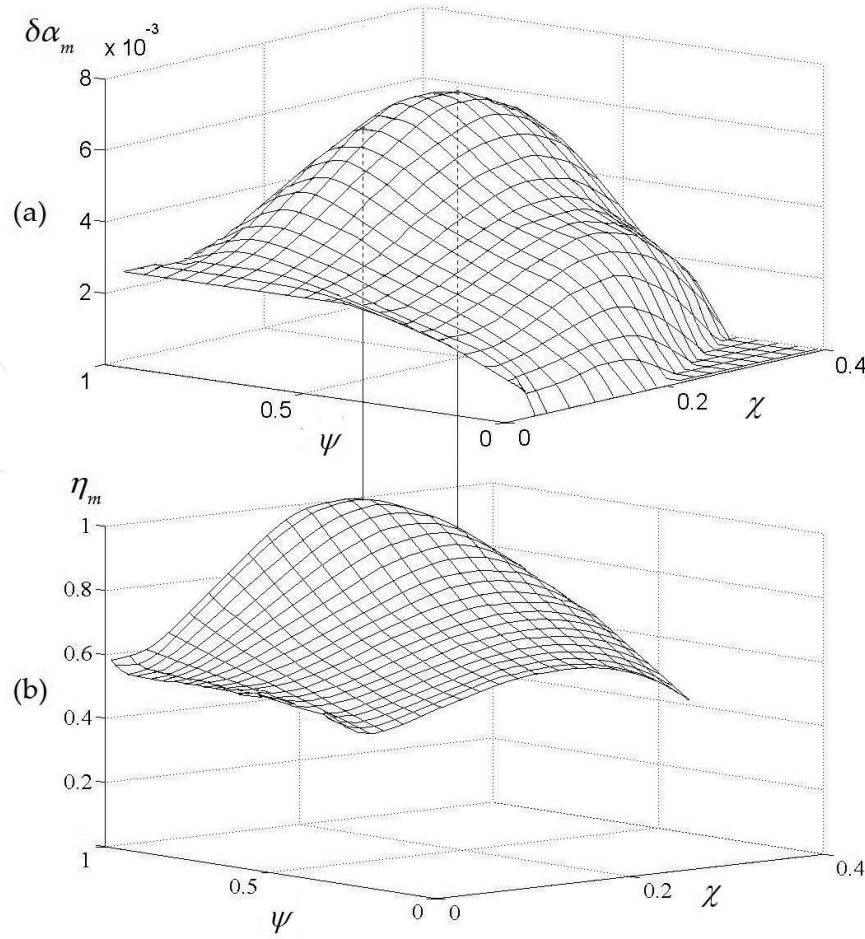


Figure 4. Angle of incidence $\delta\alpha_m$ and efficiency η_m versus the angles ψ and χ at $K_2 = 5$ for lithium niobate (LiNbO_3) crystal at $\mathbf{m}_0 \parallel \mathbf{x}_2$, $\mathbf{n}_0 \parallel \mathbf{y}$, $\mathbf{x}_2 = (\cos\theta_2, 0, \sin\theta_2)$, and $\theta_2 = 0.46$.

Figure 4 shows the optimization of the parameters $\delta\alpha_m$ and η_m for the lithium niobate crystal that corresponds to the value $K_2 = 5$ at the variation of the orientations of the normal \mathbf{n} to the surface, i.e., the angles ψ and χ . For each \mathbf{n} direction, the surface $K_2(\varphi, \delta\alpha)$ similar to that shown in **Figure 3** was plotted from which the φ_m and $\delta\alpha_m$ values corresponding to the extremal point at the “crest” with the amplitude $K_2 = 5$ were determined. Consequently, each point on the $\delta\alpha_m(\psi, \chi)$ and $\eta_m(\psi, \chi)$ surfaces in **Figure 4** corresponds to a certain angle φ_m . As is seen in the figure, the variations of the angles ψ and χ can significantly increase $\delta\alpha_m$ and η_m .

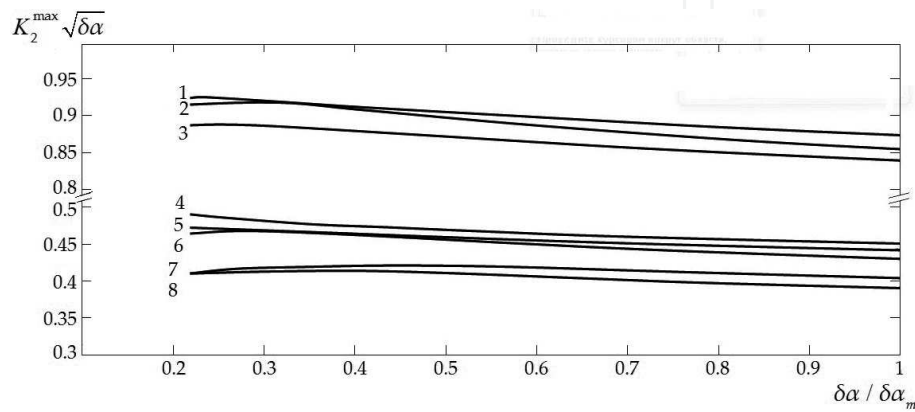


Figure 5. Numerical plot of the product $K_2^{\max} \sqrt{\delta\alpha}$ versus $\delta\alpha$ for the series of acoustic crystals (1— BaTiO_3 , 2—paratellurite, 3—graphite, 4— CdCe , 5— ZnS , 6— LiF , 7— LiNbO_3 , 8— Si).

The positions of maxima on the surfaces do not coincide but are quite close to each other, which allows a reasonable compromise at the choice of geometry.

Let us now check to what extent the found relations between parameters of our resonance reflection found in the first order of the perturbation theory retain their validity in a more precise numerical description. To be exact, we are checking the analytical dependence (28) of the extremal gain on the tuning angle $\delta\alpha$. And indeed, the numerical plot in **Figure 5** of the products $K_2^{\max} \sqrt{\delta\alpha}$ versus $\delta\alpha$ for eight analyzed acoustic crystals shows these dependences as very slowly changing functions close to constants.

6. Explicit theory for hexagonal crystals

In this section based on [11], we present the explicit analytical theory of the effect under consideration for a hexagonal medium with transversely isotropic elastic properties, which makes it possible to specify the above general relations and express the geometric conditions for mode conversion in terms of the moduli of elasticity of crystal. Analytical considerations will be supplemented with numerical calculations for some of hexagonal crystals.

To describe a hexagonal crystal, we use a standard crystallographic system of coordinates with the z axis oriented parallel to principal symmetry axis 6 and the x and y axes orthogonal to the z axis and lying in the basal plane of transverse isotropy [14, 15]. We choose the crystal boundary P_0 to be parallel to the axis 6 so that the normal \mathbf{n}_0 to this boundary is directed along the y axis. In this geometry, an EBW with the polarization $\mathbf{A}_{02} \parallel \mathbf{z}$ can propagate along the crystal surface in the direction $\mathbf{m}_0 \parallel \mathbf{x}$ with a speed:

$$\hat{v}_0 = \sqrt{c_{44}/\rho}. \quad (29)$$

For transverse isotropy, we may change the initial crystal surface orientation $P_0 \rightarrow P$, rotating its normal vector \mathbf{n} around \mathbf{m}_0 (i.e., choosing in **Figure 2a** the angle $\chi = \pi/2$) by a small angle ψ

$$\mathbf{n}_0 \rightarrow \mathbf{n} = (0, \cos \psi, \sin \psi). \quad (30)$$

In addition, as before, we introduce a perturbed propagation direction \mathbf{m} rotated relative to the vector \mathbf{m}_0 by a small angle ϕ in the new surface plane P :

$$\begin{aligned} \mathbf{m}_0 \rightarrow \mathbf{m} &= \mathbf{m}_0 \cos \phi + [\mathbf{n} \times \mathbf{m}_0] \sin \phi, \\ [\mathbf{n} \times \mathbf{m}_0] &= (0, \sin \psi, -\cos \psi). \end{aligned} \quad (31)$$

Based on the standard equations of crystal acoustics [14, 15], one can determine the wave parameters entering superposition (1)

$$\begin{aligned} \mathbf{A}_{1,4} &= (\pm p, 1, 0) \sqrt{c_{66}/c_{44}}, \\ \mathbf{L}_{1,4} &= \{2c_{66} - c_{44}, -2c_{66}p, (\pm p\psi - \phi)c_{44}\} \sqrt{c_{66}/c_{44}}, \end{aligned} \quad (32)$$

$$\begin{aligned} \mathbf{k}_{1,4} &= k(1, \pm p, -\phi); \\ \mathbf{A}_2 &= (\phi d / \Delta_{14}, 0, 1), \\ \mathbf{L}_2 &= \{\psi, \beta\phi, \delta p + \tilde{\beta}\phi\psi\} c_{44}, \\ \mathbf{k}_2 &= k(1 - \phi^2/2, \delta p + \phi\psi, -\phi); \end{aligned} \quad (33)$$

$$\begin{aligned}
 \mathbf{A}_3 &= \{1, iq, (-\varphi + iq\psi)d/\Delta_{14}\}\sqrt{c_{11}/c_{44}}, \\
 \mathbf{L}_3 &= \{2ic_{66}q, c_{44} - 2c_{66}, -c_{44}(\psi + i\kappa q\varphi)\}\sqrt{c_{11}/c_{44}}, \\
 \mathbf{k}_3 &= k(1, iq, -\varphi).
 \end{aligned} \tag{34}$$

The following designations are introduced in formulas (32)–(34):

$$p = \sqrt{\Delta_{46}/c_{66}}, \quad q = \sqrt{\Delta_{14}/c_{11}}; \tag{35}$$

$$\beta = \frac{c_{12}d - \Delta_{13}\Delta_{14}}{c_{44}\Delta_{14}}, \quad \tilde{\beta} = \frac{c_{13}d - \Delta_{34}\Delta_{14}}{c_{44}\Delta_{14}}, \quad \kappa = 1 + \frac{d}{\Delta_{14}}; \tag{36}$$

$$\Delta_{ij} = c_{ii} - c_{jj}, \quad d = c_{44} + c_{13}. \tag{37}$$

We assume the parameters q and p to be real, which holds true at $c_{11} > c_{44} > c_{66}$. Note that the inequality $c_{11} > c_{66}$ is always satisfied (this is the crystal stability condition [14]) and the inequality $c_{11} > c_{44}$ is almost always satisfied (we do not know exclusions). Meanwhile, the condition $c_{44} > c_{66}$, which indicates that EBW (29) belongs to the middle sheet of the slowness surface (**Figure 2b**), is valid in far from all crystals (say, in a half of them).

As before, the angle of incidence is chosen near the angle $\hat{\alpha}$ of total internal reflection (**Figure 2b**). This angle corresponds to the limiting speed, which now can be directly related to the EBW speed \hat{v}_0 (29):

$$\hat{v}^2 = \hat{v}_0^2(1 - \hat{\beta} \varphi^2), \quad \hat{\beta} = \frac{d^2 - \Delta_{14}\Delta_{34}}{c_{14}\Delta_{14}}. \tag{38}$$

In turn, the small tuning angle $\delta\alpha$ corresponds to the interval $\delta v = v - \hat{v}$ and, consequently, to the parameter δp :

$$\delta v = \hat{v}_0 p \delta\alpha = \frac{1}{2} \hat{v}_0 \delta p^2, \quad \delta\alpha = \delta p^2 / 2p. \tag{39}$$

Substituting expressions (32)–(34) for the vectors \mathbf{L}_α into Eq. (5), we obtain reflectances R_1 and R_2 as functions of the moduli of elasticity and perturbation parameters ϕ , ψ , and δp :

$$R_1 = \frac{\varphi^2 + ia\psi^2 - (\lambda' + i\lambda'')(\delta p + \hat{\beta} \varphi\psi)}{-\varphi^2 + ia\psi^2 - (\lambda' - i\lambda'')(\delta p + \hat{\beta} \varphi\psi)}, \tag{40}$$

$$R_2 = \frac{\mu\varphi + i\tilde{\mu}\psi}{\varphi^2 - ia\psi^2 + (\lambda' - i\lambda'')(\delta p + \hat{\beta} \varphi\psi)}, \tag{41}$$

where

$$\begin{aligned}
 a &= \frac{p}{q\beta^2}, \quad \lambda' = p\left(\frac{2c_{66}}{\beta c_{44}}\right)^2, \quad \lambda'' = \frac{1}{q}\left(\frac{2c_{66} - c_{44}}{\beta c_{44}}\right)^2, \\
 \mu &= \frac{4pc_{66}}{\beta c_{44}}\sqrt{\frac{c_{66}}{c_{44}}}, \quad \tilde{\mu} = \frac{2p(2c_{66} - c_{44})}{q\beta^2 c_{44}}\sqrt{\frac{c_{66}}{c_{44}}}.
 \end{aligned} \tag{42}$$

Taking into account Eq. (40), we can reduce the conversion condition $R_1 = 0$ to the system of equations:

$$\begin{aligned}\lambda''\varphi^2 - a\lambda'\psi^2 &= 0, \\ \varphi^2 - \lambda'(\delta p + \varphi\psi\widehat{\beta}) &= 0.\end{aligned}\quad (43)$$

The first equation yields two versions of the mode conversion relationship between the rotation angles of the boundary (ψ) and sagittal plane (ϕ):

$$\psi_{\text{con}} = \pm \gamma \varphi_{\text{con}}, \quad \gamma = \sqrt{\frac{\lambda''}{a\lambda'}}. \quad (44)$$

Substituting the parameter values from Eq. (42) into the radicand of Eq. (44), we can easily see that for $c_{44} > c_{66}$ in the case under consideration, the γ value is always real:

$$\gamma = \left| \frac{(c_{44} - 2c_{66})[c_{44}(c_{11} - 2c_{66}) + c_{13}(c_{44} - 2c_{66})]}{2c_{44}(c_{11} - c_{44})\sqrt{c_{66}(c_{44} - c_{66})}} \right|. \quad (45)$$

In other words, at $c_{44} > c_{66}$, there are always two crystal cuts, i.e., two versions of coupled orientations of the boundary and sagittal planes, which ensure mode conversion near angle $\hat{\alpha}$ of total internal reflection. Certainly, each set of chosen angles $\psi = \pm\gamma\varphi$ corresponds to its own definite angle of incidence: $\delta\alpha = \delta p^2/2p$ (39). The second equation in (43) yields:

$$\delta p_{\text{con}}^{\pm} = \varphi_{\text{con}}^2 \left(\frac{1}{\lambda'} \mp \gamma \widehat{\beta} \right), \quad \delta\alpha_{\text{con}}^{\pm} = \frac{\varphi_{\text{con}}^4}{2p} \left(\frac{1}{\lambda'} \mp \gamma \widehat{\beta} \right)^2. \quad (46)$$

Thus, the resonance width with respect to the incidence angle is indeed very small: $\delta\alpha \propto \varphi^4$. As we have seen, it is preferable to choose the sign corresponding to the maximum value $\delta\alpha_{\text{con}}^{\pm}$ (the upper sign at $\widehat{\beta} < 0$ and the lower sign at $\widehat{\beta} > 0$):

$$\psi_{\text{con}} = -\gamma\varphi_{\text{con}} \operatorname{sgn} \widehat{\beta}, \quad \delta\alpha_{\text{con}} = \frac{\varphi_{\text{con}}^4}{2p} \left(\frac{1}{\lambda'} + \gamma|\widehat{\beta}| \right)^2. \quad (47)$$

Given the found relations for reflectances (40) and (41), we can obtain the gain (K_2) and loss (K_1) coefficients (8) where one can put

$$s_1 \approx s_4, \quad s_2/s_4 \approx \sqrt{c_{44}/c_{66}}. \quad (48)$$

Here we took into account that for the studied reflection geometry with the sagittal plane close to transverse isotropy, the ray speeds s_{α} are approximately equal to the phase speeds of the bulk waves involved in the reflection. Under the total conversion conditions (44)–(47), the coefficient K_1 is 0; therefore, the excitation efficiency of beam r_2 is maximum: $\eta = 1 = 100\%$. In this case, the gain K_2 can be written as:

$$K_2^{\text{con}} = \frac{G_{\text{con}}}{\varphi_{\text{con}}^2}, \quad G_{\text{con}} = \frac{(\mu^2 + \tilde{\mu}^2\gamma^2)s_2/s_4}{4(1 + a^2\gamma^4)}. \quad (49)$$

The above analysis based on expansion of the equations in small parameters φ^2 , ψ^2 , δp , and $\delta\alpha$ is approximate. Therefore, the range of applicability of the results obtained may differ, depending on the degree of crystal anisotropy and other factors. In **Figure 6**, the analytical linear relation between the conversion angles φ

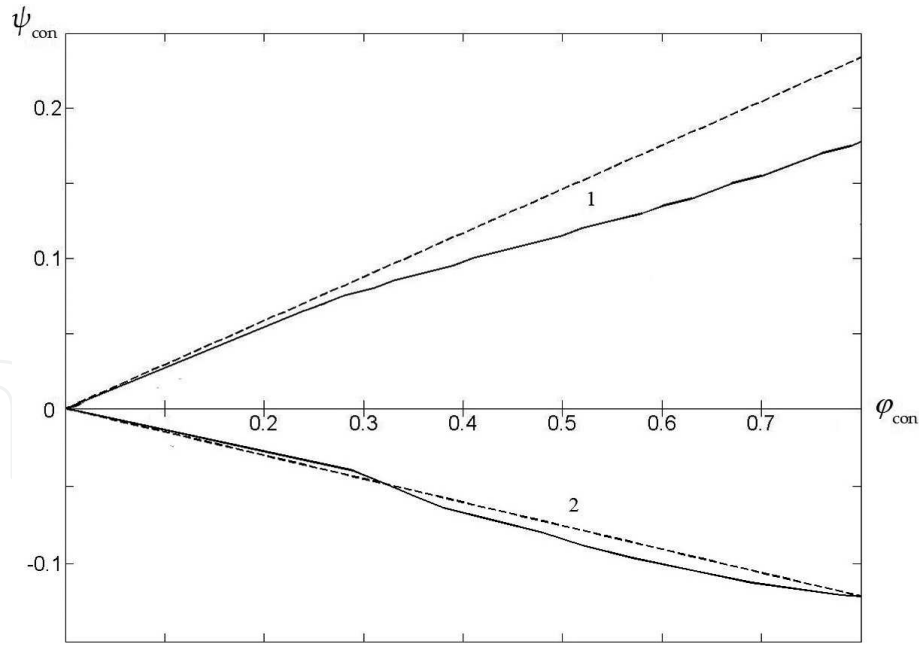


Figure 6.

Correlations between the conversion angles ψ_{con} and ϕ_{con} (in radians) obtained by numerical calculation (solid lines) and approximate theoretical analysis (dashed lines) for the (1) Ti and (2) BeCu crystals.

and ψ (47) is compared with the results of numerical calculations based on formulas (5), without their expansion in small parameters, on the example of two (Ti, and BeCu) hexagonal crystals [16, 17].

In both cases, our computations not only practically confirm linearity of the relation between ϕ and ψ but also yield slopes of these dependences close to theoretical ones. In case of Ti, we have $\hat{\beta} < 0$ and coincident signs of angles ϕ and ψ , while for BeCu, $\hat{\beta} > 0$ and the angle signs are different.

We can only wonder why the predictions in the first order of the perturbation theory are confirmed so well by the exact numerical calculation in a wide range of angles ϕ , which are far from small. Anyhow, but the Ti crystal reveals one more “loyalty” with respect to our approximate theory: in its case, the geometries of the mode conversion and the extremal gain are almost identical.

7. The particular case of 1D perturbation ($\psi = 0$)

The presented theory of mode conversion in the vicinity of the angle of total internal reflection was based on coupled perturbations of both the sagittal plane and the surface orientations. At the rotations of only one of these planes, the mode conversion can be achieved only for crystals with certain relations between the moduli of elasticity. However, sometimes, these requirements might appear to be not very limiting. This can be explicitly shown on the example of the considered above case of hexagonal crystals. Indeed, for the unperturbed surface at $\psi = 0$, the loss coefficient K_1 (40) acquires a minimal value K_1^{\min} at $\varphi^2 = \lambda' \delta p$ which may be estimated as:

$$K_1^{\min} = |R_1|^2 = \left| \frac{\lambda''}{2\lambda'} \right|^2 \sim \left(\frac{c_{44} - 2c_{66}}{c_{44}} \right)^4. \quad (50)$$

Thus, any hexagonal crystal with the modulus c_{44} close to $2c_{66}$ must be very efficient for our effect ($K_1 \ll 1$). Due to the “4” power in the latter estimate, this remains

true even when the moduli are not so close to each other. For instance, at $|c_{44} - 2c_{66}|/c_{44} \sim 1/3$, Eq. (50) gives the estimate $K_1 \sim 10^{-2}$ and efficiency $\eta = 1 - K_1$ becomes $\sim 99\%$. In accordance with reference book [16], there are quite a number of hexagonal crystals where $K_1 \ll 1$. Below, we shall also give examples of crystals of monoclinic symmetry systems having got the same property.

This motivates us to a short consideration of the simplified approach to the reflection resonance with unchanged crystal surface orientation. As was shown in [8], the description becomes especially compact if to choose the crystal boundary parallel to the plane of crystal symmetry. By the way, such planes exist in all crystals, except triclinic [14, 15]. In this case, expressions (21) and (22) acquire the structure:

$$K_1 = \frac{(\varphi^2 - \lambda' \delta p)^2 + (\lambda'' \delta p)^2}{(\varphi^2 + \lambda' \delta p)^2 + (\lambda'' \delta p)^2}, \quad (51)$$

$$K_2 = \frac{(\mu \varphi)^2 s_2 / s_4}{(\varphi^2 + \lambda' \delta p)^2 + (\lambda'' \delta p)^2}. \quad (52)$$

And the efficiency of the resonance $\eta = 1 - K_1$ is given by:

$$\eta = \frac{4\lambda' \delta p \varphi^2}{(\varphi^2 + \lambda' \delta p)^2 + (\lambda'' \delta p)^2}. \quad (53)$$

Thus, for a fixed δp , the coefficients K_2 and η are determined by the same function $F(\varphi)$:

$$K_2(\varphi) = \frac{\mu s_2}{s_4} F(\varphi), \quad \eta(\varphi) = 4\lambda' \delta p F(\varphi), \quad F(\varphi) = \frac{\varphi^2}{(\varphi^2 + \lambda' \delta p)^2 + (\lambda'' \delta p)^2}. \quad (54)$$

Accordingly, their maximum magnitudes are determined by the same extremum condition:

$$\varphi^2 = |\lambda| \delta p = \delta p \sqrt{\lambda'^2 + \lambda''^2} \approx \lambda' \delta p \left[1 + \frac{1}{2} \left(\frac{\lambda''}{\lambda'} \right)^2 \right]. \quad (55)$$

The last estimate in (55) is valid when $(\lambda''/\lambda')^2 \ll 1$. In this approximation, one obtains

$$K_1^{\min}(\varphi, \delta \alpha) \approx \left(\frac{\lambda''}{2\lambda'} \right)^2, \quad K_2^{\max}(\varphi, \delta \alpha) \approx \frac{G}{\varphi^2}, \quad G \approx \frac{\mu s_2}{s_4}. \quad (56)$$

Thus, one can conclude that the consistent variation of the sagittal plane orientation φ and the tuning incidence angle $\delta \alpha \propto \delta p^2$ (10) along one extremal trajectory (55) provides simultaneous optimization of both the gain and the efficiency of the resonance reflection. However, as was shown above, this coincidence is not an exact result but a consequence of our approximate calculations. The computer analysis based on exact formulas (5) without their expansion in small parameters leads to distinct extremal trajectories for the functions $K_2^{\max}(\varphi, \delta \alpha)$ and $\eta^{\max}(\varphi, \delta \alpha)$. A difference between them depends on angle φ and crystal anisotropy. On the other hand, as was discussed above, the occurrence of those trajectories might be used for

substantial increasing of the width of the resonance in the range of tuning incidence angle $\delta\alpha$ at the expense of a slight decrease in the efficiency η .

Figure 7 shows dependences $K_2(\delta\alpha)$ and $\eta(\delta\alpha)$ in such extremal trajectories related to ridges on the surfaces $K_2(\varphi, \delta\alpha)$ and $\eta(\varphi, \delta\alpha)$ (of the type shown in **Figure 3**) conformably to a monoclinic stilbene crystal. The upper curves correspond to the choice of $\varphi = f_{K,\eta}(\delta\alpha)$ in the “proper” trajectory corresponding to the maximum of the shown characteristic, while the lower curves are plotted for $\varphi = f_{\eta,K}(\delta\alpha)$ from the “foreign” trajectory. In this case, of the two possible optimization variants, the trajectory in which K_2^{\max} is realized is more advantageous. This corresponds to curves 1 in **Figure 7**. Obviously, for such a choice in the stilbene case, there is approximately only a 2.5% loss in efficiency, but in the return gain, twice in the resonance width: the value of $\delta\alpha_m$ for the optimal angle of incidence corresponding to an amplitude of $K_2^{\max} = 5$ increases from 0.08 to 0.155 rad.

In [8], we accomplished the numerical search of crystal candidates for possible future observations of the discussed effect. In all cases, the surface was supposed to be parallel to the symmetry plane while the sagittal plane orientation varied. The “casting” involved about 350 crystals. The basic criteria for the crystal selection were the closeness of the resonance to mode conversion and not too small resonance widths over the angles of incidence ($\delta\alpha_m \geq 0.01$ rad for $K_2 = 5$). According to such criteria, we found 14 crystals of monoclinic, trigonal, orthorhombic, and hexagonal systems. They are characterized by a rather high efficiency η_m , while the width $\delta\alpha$ of resonances over the angles of incidence satisfies the formulated selection rule. The resulting parameters of the resonance in these crystals are described in [8].

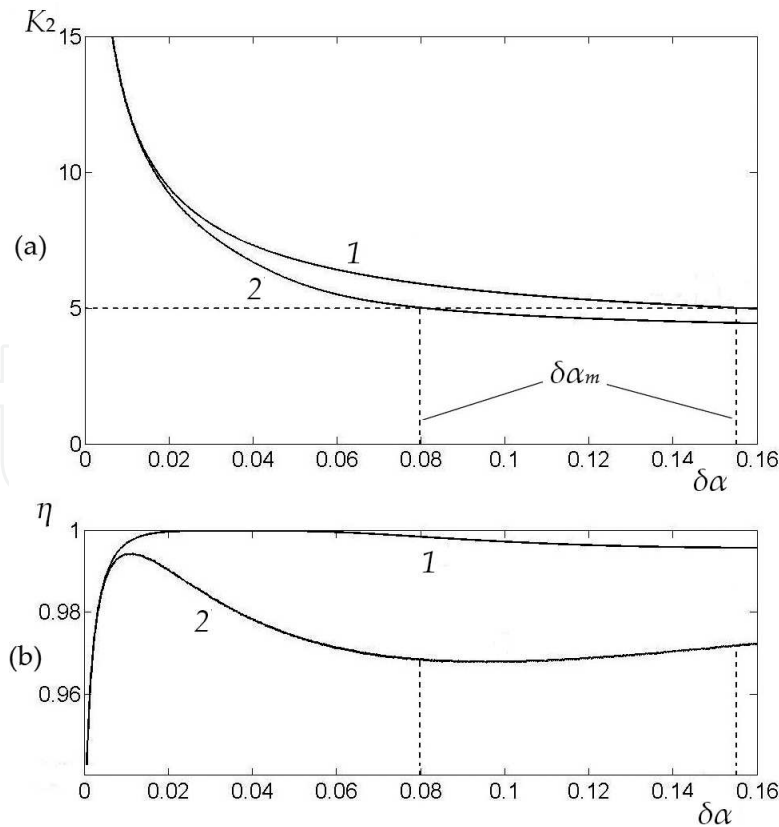


Figure 7.

Dependences of the gain coefficient K_2 (a) and the efficiency η (b) of the resonance on the incidence angle $\delta\alpha$ in a stilbene crystal with the surface parallel to the symmetry plane for optimal trajectories corresponding to the “ridges” of surfaces $K_2(\varphi, \delta\alpha)$ (curves 1) and $\eta(\varphi, \delta\alpha)$ (curves 2).

Crystals	φ_0 , rad	φ_m , rad	$\delta\alpha_m$, rad	η_m , %
Stilbene	1.54	−0.16	0.155	97.2
Triglycine sulfate	1.35	0.12	0.089	91.0
Benzyl	1.03	0.73	0.069	97.6
Tartaric acid	−1.13	−0.30	0.021	97.4

The directions of \mathbf{m}_0 are specified by the azimuth angles φ_0 counted from the x axis of the crystallographic coordinates and the angles φ_m —From \mathbf{m}_0 .

Table 2.
Key parameters of 1D resonance for a series of monoclinic crystals.

Here, we limit ourselves to presenting only data for several monoclinic crystals with the best parameters (see **Table 2**). The values of $\delta\alpha_m$, φ_m , and η_m presented in the table for all crystals correspond to the same gain $K_2 = 5$ and relate to the choice of optimal trajectory φ_K as for stilbene (**Figure 7**). This results in the maximum width of resonance for a small decrease in efficiency η_m . By the way, stilbene is the absolute leader in the table in the value of $\delta\alpha_m$ and one of the leaders in the efficiency η_m .

8. Conclusions

The analytical theory developed above is constructed within the theory of elasticity and, within the range of its applicability, it is exact to the extent of Eqs. (5) and (8), which express the resonant reflection coefficients for an arbitrary anisotropic medium in terms of the eigenvectors of Stroh’s matrix (3). Generally, the dependence of these eigenvectors on the geometrical parameters of reflection can easily be found by numerical methods. An analytical alternative is to expand the exact formulas (5) into a series in small angular parameters. Finally, an explicit analytical calculation based on these formulas for a number of geometries in high-symmetry crystals (for example, hexagonal ones) is also possible. Here, we used all three approaches: the numerical calculations based on Eqs. (5) and (8), their expansion into a series, and even an explicit representation of the results via the elastic moduli. In this case, avoiding the cumbersomeness of our calculations and the unmanageability of the analytical formulas, we retained only the first non-vanishing terms in all expansions that conveyed the key dependences and the effect being investigated on physical parameters. On the other hand, all graphical results of our analysis were obtained through computations based on the exact formulas (5) and (8).

Based on the same principles, we used the image of acoustic beams in our reasoning only for clarity. Actually, we did not go outside the plane wave approximation in our calculations by assuming it to be sufficient in the short wavelength limit of interest, $\lambda/D \sim 10^{-3}$ rad. Here, we also had in mind the possible manifestations of the effect in phonon physics, where the language of plane waves is more relevant.

Based on our analysis, we can probably count on the realization of resonant reflection in crystals, whereby a wide incident acoustic beam converts almost all of its energy into a narrow high-intensity reflected beam. A special choice of crystals with a definite relation between the elastic moduli is required to optimize the resonance. In addition, since the resonance region is narrow in angles of incidence,

stringent requirements for a weak divergence of the incident beam, $\sim 10^{-3}$ rad, which can be realized only at high ultrasonic frequencies ~ 100 MHz, arise. For the same reason, the amplitude of the excitation coefficient is also limited to $K_2 \approx 5\text{--}10$. However, in the case of retransformation of the emergent beam through its narrowing in the perpendicular dimension as well, the intensification efficiency increases many fold, to $\sim 10^2$. In the hypersonic frequency range, the amplification amplitudes can be increased significantly. In this case, however, one might expect additional restrictions due to an increase in the absorption of acoustic waves.

The acoustic resonance considered here can also manifest itself in phonon physics as the channeling of high-density energy near the surfaces of crystals with specially chosen orientations and in accompanying nonlinear phenomena. The strategy for an experimental search of such effects can be based on existing techniques for studying the manifestations of phonon focusing [3] and the propagation of ballistic phonons [18].

Acknowledgements


This work was supported in part by the Ministry of Education and Science of the Russian Federation (state assignment for Federal Research Center “Crystallography and Photonics”).

Author details

Vladimir I. Alshits*, Dmitrii A. Bessonov and Vasilii N. Lyubimov
A.V. Shubnikov Institute of Crystallography, Federal Research Center
“Crystallography and Photonics,” Russian Academy of Sciences, Moscow, Russia

*Address all correspondence to: valshits@mail.ru

IntechOpen

© 2018 The Author(s). Licensee IntechOpen. This chapter is distributed under the terms of the Creative Commons Attribution License (<http://creativecommons.org/licenses/by/3.0>), which permits unrestricted use, distribution, and reproduction in any medium, provided the original work is properly cited. 

References

- [1] Royer D, Dieulesaint E. Elastic Waves in Solids. Vol. 1, 2. Berlin: Springer; 2000. DOI: 10.1007/978-3-642-02589-1
- [2] Aleksandrov KS, Sorokin BP, Burkov SI. Effective Piezoelectric Crystals for Acoustoelectronics, Piezotechnics and Sensors. Vol. 1, 2. Novosibirsk: Sib. Otd. RAN; 2007-2008
- [3] Wolfe JP. Imaging Phonons. Cambridge, UK: Cambridge University Press; 2005
- [4] Ponomarev AE, Bulatitskii SI, Sapozhnikov OA. Compression and amplification of an ultrasonic pulse reflected from a one-dimensional layered structure. *Acoustical Physics*. 2007;**53**:127-135. DOI: 10.1134/S1063771007020030
- [5] Alshits VI, Bessonov DA, Lyubimov VN. Resonant excitation of intense acoustic waves in crystals. *Journal of Experimental and Theoretical Physics*. 2013;**116**:928-944. DOI: 10.1134/S1063776113060010
- [6] Chadwick P, Smith GP. Foundations of the theory of surface waves in anisotropic elastic materials. *Advances in Applied Mechanics*. 1977;**17**:303-376. DOI: 10.1016/S0065-21560870223-0
- [7] Alshits VI, Lothe J. Elastic waves in triclinic crystals. I. General theory and the degeneracy problem. *Soviet Physics Crystallography*. 1979;**24**:387-392
- [8] Alshits VI, Bessonov DA, Lyubimov VN. Resonance compression of an acoustic beam in a crystal. *Journal of Experimental and Theoretical Physics*. 2016;**122**:689-704. DOI: 10.1134/S1063776116020151
- [9] Alshits VI, Bessonov DA, Lyubimov VN. Excitation of intense acoustic waves in hexagonal crystals. *Crystallography Reports*. 2013;**58**:867-876. DOI: 10.1134/S1063774513060047
- [10] Alshits VI, Bessonov DA, Lyubimov VN. Intensification of acoustic beams in crystals at mode conversion near total internal reflection. *JETP Letters*. 2017;**106**:40-45. DOI: 10.1134/S0021364017130069
- [11] Lyubimov VN, Bessonov DA, Alshits VI. Compression of acoustic beams at conversion reflection in hexagonal crystals. *Crystallography Reports*. 2018;**63**:621-626. DOI: 10.1134/S1063774518040168
- [12] Stroh AN. Steady state problems in anisotropic elasticity. *Journal of Mathematical Physics*. 1962;**41**:77-103
- [13] Barnett DM, Lothe J. Free surface (Rayleigh) waves in anisotropic elastic half-spaces: The surface impedance method. *Proceedings of the Royal Society of London*. 1985;**A402**:135-152
- [14] Fedorov FI. *Theory of Elastic Waves in Crystals*. New York: Plenum Press; 1968 (Moscow: Nauka; 1965)
- [15] Sirotin Yu I, Shaskolskaya MP. *Fundamentals of Crystal Physics*. Moscow: Mir; 1982
- [16] Landolt HH, Börnstein R. In: Hellwege K-H, editor. *Zahlenwerte und Funktionen aus Naturwissenschaften und Technik*. 11th ed. Vol. Neue Serie, III. Berlin: Springer; 1979
- [17] Blistanov AA, Bondarenko VS, Perelomova NV, et al. *Acoustic Crystals: A Handbook*. Moscow: Nauka; 1982

[18] Alshits VI, Ivanov SN, Soifer Ya M, Taranov AV, Khazanov EN. The observation of dislocation flutter-resonance in the temperature dependence of scattering of nonequilibrium phonons in LiF crystals. *Soviet Physics—Solid State*. 1989;**31**:1873-1879

IntechOpen

IntechOpen